Hydroacoustic Modeling of Rotor Stator Interaction in Francis Pump-Turbine

Nicolas RUCHONNET

EPFL Lausanne, Swizerland, nicolas.ruchonnet@epfl.ch

Christophe NICOLET

EPFL Lausanne, Swizerland, christophe.nicolet@epfl.ch

François Avellan

EPFL Lausanne, Swizerland, francois.avellan@epfl.ch

ABSTRACT

A one-dimensional hydroacoustic model is set up to perform the numerical simulation of the rotor-stator interaction of a Francis pump-turbine scaled model. The numerical results enable to identify both rotating diametrical modes in the vaneless gap between the 20 guide vanes interacting with the 9 rotating impeller blades and the standing waves in the spiral casing. Moreover, the simulations enlighten the interaction between these rotating diametrical modes and the standing waves.

INTRODUCTION

Hydraulic pump-turbine operating under steady state conditions are subject to pressure fluctuations resulting from the interaction of the rotating parts and the stationary parts of the machine. This Rotor-Stator Interaction, RSI, are the

consequence of the interaction between the rotating flow perturbations so-called potential flow perturbations caused by the impeller blades and the flow perturbation caused by the guide vanes. This interaction induces pressure waves propagating in the entire hydraulic machine. As a result the RSI phenomena may cause two different kinds of pressure fluctuations in the machine:

- Diametrical pressure mode rotating in the vaneless gap between the guide vane and the impeller blades as described by Bolleter [1] and Tanaka et al. [2];
- Standing waves in the spiral casing as described by Chen [3]and Dörfler [4].

The first phenomenon may cause hydromechanics resonance between the rotating diametrical pressure mode and the structure of impeller [5] or of the head cover [6] and may induce strong vibrations, noise, fissures or guide vanes bearing ruins. The second phenomenon may cause resonance with the power house structure that generates unacceptable vibrations and noise [2]. The standing wave phenomenon may affect also the penstock [4], [7] which evidences the potential interaction of the hydraulic machine with the hydraulic circuit.

The prediction of such phenomena is a challenging task during the early stage of the design of a reversible pump turbine unit for a hydroelectric power plant. Some analytical models have been developed by Bolleter [1] and Tanaka and al. [2] for the diametrical mode shape and by Chen [3] and Dörfler [4] for the standing wave allowing for the prediction of the risk of occurrence of these phenomena. The prediction of the occurrence of the standing wave is based on the analysis of the traveling time of pressure waves propagating in a one-dimensional system modeling the pump turbine accordingly to its topology. Recently, Haban et al. [8] have developed more sophisticated one-dimensional models based on matrix transfer method that have shown their capability of predicting spiral casing standing wave patterns. By the use of such models Fischer et al. [6] have pointed out the link between the standing waves in the spiral casing and the penstocks and the

diametrical pressure mode rotating in the vaneless gap by performing a forced response analysis in the frequency domain. However this approach requires the identification of the excitation pattern by the method described by Bolleter [1] and Tanaka et al. [2].

The simulation of the incompressible 3D unsteady flow of a vaneless centrifugal pump performed by Gonzalez et al. [9] using commercial CFD tool has shown the capability of CFD to predict accurately the unsteady convective field related to the RSI phenomenon at the blade passing frequency which is dominant close to the nominal operating point. However some discrepancies appeared for off-design operating conditions where acoustic behavior becomes more effective due to a blade-tongue interaction. Such an incompressible code cannot account for the propagating part of the flow which may lead to standing wave phenomenon. Therefore the separation of hydraulic and acoustic pressure fluctuations by means of least-squares residual method developed by Morgenroth [10] was used. A model accounting for both the jet-wake pattern of the convective flow and for the blade-tongue interaction has been set up by Parrondo et al. [11]. Through an experimental identification of the parameters of acoustic model a good agreement has been found between the model and the measurements even for off-design operating conditions where the amplitude of the blade-tongue interaction was found to have 10 times the amplitudes of the wake jet part of the flow.

To be able to predict the amplitudes of the pressure fluctuations resulting from RSI it appears that combination of unsteady incompressible RANS model and 1D acoustic model is a suitable approach. This approach would leads to a RSI computing methodology for the prediction of pressure amplitudes where the unsteady incompressible RANS calculation accounts for the rotor stator excitation mechanism considering all the parameters; i. e. vaneless gap, impeller blade angle, guide vane opening, jet-wake effect, etc. The first step of this approach is to set up a

hydroacoustic model of a pump turbine and to investigate RSI patterns and perform a sensitivity study of the model.

This paper aims to present the numerical simulation of the hydroacoustic part of the RSI phenomenon based on a one-dimensional hydroacoustic model. Therefore the case of 20 guide vanes and 9 impeller blades high head Francis pump turbine is investigated. First the RSI patterns of the pump turbine are described. Then the mathematical model implemented in the software SIMSEN is briefly presented. The determination of the pump turbine hydroacoustic parameters is described. The RSI excitation is modeled by a valve network driven accordingly to the spatial and temporal evolution of the flow distribution between the stationary and the rotating parts of the machine. The results obtained by the simulations in time domain evidences the RSI patterns of the pump turbine of interest.

RSI PATTERNS IN FRANCIS PUMP TURBINE

The flow field leaving the guide vane of a Francis pump turbine in generating mode is characterized by the velocity defect caused by the guide vanes. The pressure field attached to the rotating impeller blade induces also incoming flow field distortions. No matter how complex are these two periodic flow fields they can be expressed as Fourier series. Then, both the stationary and rotating pressure fields can be expressed as:

$$p_s(\theta_s,t) = \sum_{n=1}^{\infty} B_n \cos\left(nZ_0\theta_s + \phi_n\right) \quad p_r(\theta_r,t) = \sum_{m=1}^{\infty} B_m \cos\left(mZ_b \cdot \theta_r + \phi_m\right) \quad \text{(1) and (2)}$$

The resulting pressure field, combining the guide vanes and the impeller blade pressure field is characterized by a strong modulation process as illustrated Figure 1. The pressure in the area of the vaneless gap between the guide vanes and impeller blades can therefore be expressed as the product of both rotating and stationary fields of pressure leading to the summation of every p_{mn} component:

$$p_{mn}(\theta, t) = A_{mn} \cos\left(nZ_o \cdot \theta_s + \phi_n\right) \cdot \cos\left(mZ_b \cdot \theta_r + \phi_m\right) \text{ for } n = 1, 2, \ldots \infty \text{ and } m = 1, 2, \ldots \infty \quad (3)$$

Where A_{mn} is the combined pressure amplitude due to the interaction of each harmonics [2]. By using the well known identity for circular functions: Eq.(3) can be expressed as:

$$p_{mn}(\theta_s, t) = \frac{A_{mn}}{2} \cos\left(nZ_o \cdot \theta_s - mZ_b \cdot \theta_r + \phi_n - \phi_m\right) + \frac{A_{mn}}{2} \cos\left(nZ_o \cdot \theta_s + mZ_b \cdot \theta_r + \phi_n + \phi_m\right) \quad (4)$$

Moreover, the impeller angle coordinate is related to the stationary system of reference as $\theta_r = \theta_s - \omega t$, then the pressure field in the stationary coordinates becomes:

$$p_{mn}(\theta_s, t) = \frac{A_{mn}}{2} \cos\left(mZ_b \omega t - \left(mZ_b - nZ_o\right)\theta_s + \phi_n - \phi_m\right)$$
$$+ \frac{A_{mn}}{2} \cos\left(mZ_b \omega t - \left(mZ_b + nZ_o\right)\theta_s - \phi_n - \phi_m\right) \quad (5)$$

Flow field distortion due to runner pressure field

Flow field distortion due to guide vane wake

Combination of both effects

Figure 1 Modulation process between impeller blade flow field and guide vanes flow field.

This equation describes the RSI pressure field in the vaneless gap which is function of time and space [12]. This pressure field represents 2 diametrical pressure modes having the following numbers of minima and maxima :

$$k_1 = m \cdot Z_b - n \cdot Z_o \text{ and } k_2 = m \cdot Z_b + n \cdot Z_o \quad (6)$$

rotating with the respective spinning speed in the stationary frame of reference.

$$\omega_1 = mZ_b \omega_b / k_1 \text{ and } \omega_2 = mZ_b \omega_b / k_2. \quad (7)$$

Furthermore, the sign of the diametrical mode numbers k_1 and k_2 indicates that the diametrical mode is rotating in the same direction as the impeller when positive and

counter-rotating when negative. It is also important to notice that lower amplitudes are expected for higher k values, because of the high harmonic number. As a result, k_2 is usually not relevant. The Figure 2 presents an illustration of the meaning of the k values.
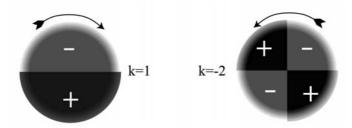

Figure 2 Diametrical modes shapes representation according to k values.

The pump turbine of interest is a scale model of pump turbine which has a specific speed of $\nu = 0.17$, 20 guide vanes, 9 impeller blades and an outlet diameter (turbine mode) of $R_{1e} = 400 \text{ mm}$. According to this rotor-stator blade arrangement the RSI patterns of this pump turbine are determined analytically using relations (5), (6) and (7), see Table 1.

Table 1 RSI patterns of the pump turbine (Z_o = 20 ; Z_b = 9).

				Stationnary frame			Rotating frame		
n	m	$k1$	$k2$	ω_1 / ω_b	ω_2 / ω_b	f / f_b	$\omega_2 '/ \omega_b$	$\omega_2 '/ \omega_b$	f / f_b
		$mZ_b - nZ_o$	$mZ_b + nZ_o$	$mZ_b / k1$	$mZ_b / k2$	mZ_b	$nZ_o / k1$	$nZ_o / -k2$	nZ_o
1	2	-2	38	-9.0	0.5	18	-10.0	0.5	20
1	3	7	47	3.9	0.6	27	2.9	0.4	20
2	4	-4	76	-9.0	0.5	36	-10.0	0.5	40
2	5	5	85	9.0	0.5	45	8.0	0.5	40

Table 1 points out the 4 diametrical rotating modes shapes that may present high amplitudes, it is for $k_1 = -2, 7, 5, -4$ with the corresponding frequencies in the stationary frame $f / f_b = mZ_b = 18, 27, 36$ and 45. In the rotating frame of reference

these frequencies reduced to $f/f_b = mZ_o = 20$ for the first 2 modes and $f/f_{bo} = 40$ the second 2 modes.

Hydroacoustic Modeling of Francis Pump Turbine

Hydroacoustic modeling

By neglecting the convective terms $C\,\partial/\partial x$ and assuming plane pressure wave and uniform velocity field in a cross section, the momentum and the continuity equations established for the pipe of a length dx, a cross section A and a wave speed a, Figure 3, reduces to the simple hyperbolic partial differential equations see [13] :

$$\begin{cases} \dfrac{\partial h}{\partial t} + \dfrac{a^2}{gA} \cdot \dfrac{\partial Q}{\partial x} = 0 \\[2mm] \dfrac{\partial h}{\partial x} + \dfrac{1}{gA} \cdot \dfrac{\partial Q}{\partial t} + \dfrac{\lambda |Q|}{2gDA^2} \cdot Q = 0 \end{cases} \qquad (8)$$

Where the h and Q variables are respectively the piezometric head and the discharge expressed as:

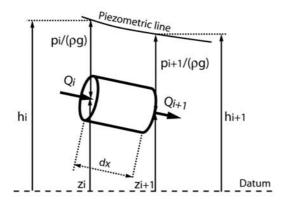$$h = z + p/(\rho \cdot g) \qquad Q = C \cdot A \qquad (9)$$

Figure 3 Pipe with a length dx.

The system of hyperbolic equations (8) is solved using Finite Difference Method considering a 1st order centered scheme discretization in space and a scheme of Lax for the discharge. This approach leads to a system of ordinary differential equations

that can be represented as a T-shaped equivalent scheme as presented Figure 4. The RLC parameters of this equivalent scheme are given by:

$$R_h = \frac{\lambda \cdot |\overline{Q}| \cdot dx}{2 \cdot g \cdot D \cdot A^2} \qquad L_h = \frac{dx}{g \cdot A} \qquad C_h = \frac{g \cdot A \cdot dx}{a^2} \quad (10)$$

Here λ is the friction coefficient. The hydraulic resistance R_h, the hydraulic inductance L_h, and the hydraulic capacitance C_h correspond respectively to losses, inertia and storage effects.

The model of pipe with a length L is made of a series of n_b elements based on the equivalent scheme of Figure 4 [14]. The system of equations relative to this model is set-up using Kirchoff laws. Time integration of the full system is achieved by a Runge-Kutta 4th order procedure.
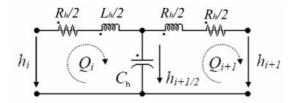

Figure 4 Equivalent scheme of a pipe.

All the procedures for building up, solving and anaylsisng the hydroacoustic model of the whole system are implemented within the in house code SIMSEN [15]. Moreover, SIMSEN provides a complete object library including both electrotechnical, control and hydraulic components such as valve, surge tanks, turbines.

Pump turbine hydroacoustic model

The plan view of the 20 guide vanes and 9 blades Francis pump turbine scale model of interest is presented Figure 5. The hydroacoustic model of this pump turbine is made of a pipe network, Figure 5.
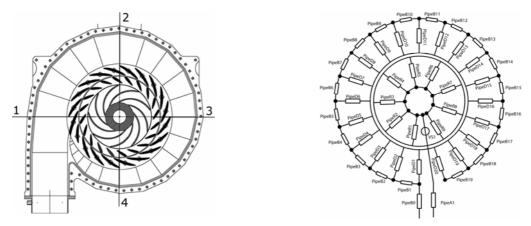
Figure 5 Plan view of the pump turbine(left) and hydroacoustic model of the pump turbine(right).

The hydroacoustic model is made of 20 pipes for the guide vanes (pipes D1 to D20), 9 pipes for the impeller (pipes R1 to R9) as well as 19 pipes for the spiral casing (pipes B1 to B19). The first part of the spiral casing between the turbine inlet and the guide vane N°1 is modeled by the pipe B0. The diffuser of the pump turbine is modeled by the pipe A1. The energy transfer through the impeller is modeled by the pressure "source" VS1 which head is function of discharge H=H(Q) according to the slope of the pump turbine characteristics linearized around the operating point of interest. The connection between the stationary part and the rotating part is achieved through 180 valves connecting each guide vane to each impeller vane. The 180 valves are controlled by the flow distribution between the stationary part and the rotating part according to the impeller angular position $\theta(t)$ The valve head loss is calculated to ensure the idealized discharge evolution presented Figure 6.
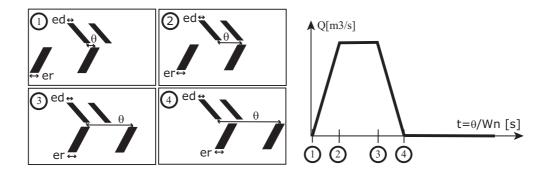

9

Figure 6 Idealized discharge evolution between a impeller vane and a guide vane as function of the spatial coordinate of the impeller θ.

Assuming a constant impeller speed the discharge evolution between one guide vane and one impeller vane is function of the connection area between them. During the rotation of the impeller 4 phases are identified:

- Phase 1: the impeller blade start to pass in front of the first blade of a guide vane, the discharge between the guide vane and the impeller vane increases linearly accordingly to the connection area increase until the impeller blade reaches the second blade of the guide vane;

- Phase 2: the discharge between the guide vane and the impeller vane remains constant until the second impeller blade reaches the first blade guide vanes, the connection area being constant;

- Phase 3: the discharge between the guide vane and the impeller vane decreases linearly according to the connection area decrease;

- Phase 4: the discharge between the guide vane and the impeller vane is kept to zero as the connection area is zero until the phase 1 is reached again.

The discharge evolution described above acts like a sliding slot between the 20 guide vanes and one impeller vane. As a result there are 9 slots for the full pump turbine, one for each impeller vane. Each slot angle being shifted by $2\pi/Z_o$. The discharge law can be modified in order to take into account the thickness of both the guide vanes and impeller blades, e_o and e_b respectively. The thickness can be expressed as equivalent angle measured in degrees at the vaneless gap radius. For the first part of investigations of this paper, the thickness of the impeller blades is taken arbitrary equal to 4°, the real one being 3°. The consideration of the blades thickness induces discontinuity in the overall discharge law. It means that the point 3 of the discharge law of an impeller blade does not correspond to the point 2 of the following

impeller blade but is shifted of the value of e_b. The lack of discharge between two consecutives impeller blades is the source of the excitation mechanism of this RSI model.

Hydroacoustic Parameters Determination

For the determination of the RLC terms of the hydroacoutic model of a pipe the following values must be determined for each pipe:

- The length, L;
- The cross section area, A;
- The friction coefficient, λ;
- The wave speed, a.

The determination of the length and cross section has been done using the structural characteristics of the pump turbine scale model. The friction coefficient of the pipes has been evaluated to be $\lambda = 0.02$ for all the pipes. The determination of the wave speed is described below.

Wave speed determination
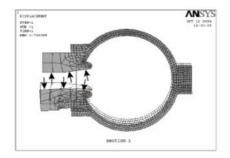
The wave speed a for the pipe is given by:

$$a^2 = \left[\rho \left(\frac{1}{E_{\text{fluid}}} + \frac{1}{A} \frac{\Delta A}{\Delta p} \right) \right]^{-1} \quad (11)$$

Where ρ is the water density, E_{fluid} is the bulk modulus of the water and $A^{-1}\Delta A / \Delta p$ is the rated area increase due to pressure increase. This term can be determined analytically for circular pipes but has to be estimated for pipes having complex cross section. In the case of the pump turbine, the wave speeds of the spiral casing and of the distributor are estimated using Finite Element Method -FEM- calculations. The determination of the wave speed of a given cross section of the spiral casing is done in two steps as presented Figure 7:

- Distributor channel area increase by assuming a constant pressure in the distributor channel only;

- Spiral casing area increase by assuming constant pressure in the spiral casing only.

The FEM analysis is made with the commercial code ANSYS™. First, stay vanes and assembling bolts are considered individually to determine their stiffness. Then, by assuming that each spiral casing part of concern is axisymmetrical, the area increase is determined by including the stiffness of the stay vanes and of the bolts previously determined.

The number of cells in the radial direction of the spiral casing section was set to 3 cells of mesh. This value was determined by comparison of circular pipe wave speed determined by both FEM and analytical calculation. The difference for such geometry was found to be 0.1%. The mechanical properties for the materials of the spiral casing and distributor channels are summarized Table 2.
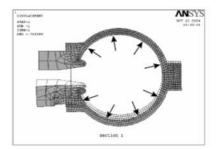

Figure 7 Determination of the wave speed in the distributor channel (left) and in the spiral casing (right).

The spiral casing materials is a composite made of Epoxy resin matrix and glass fiber. The equivalent Young modulus is calculated according to the volume fraction of both components of the composite and by taking into account the main stress direction corresponding to the uniform loading of the hydrostatic pressure. Therefore,

the glass fiber Young modulus is calculated according to the fiber cross section area and density corresponding to the main stress direction of concern.

Table 2 : Mechanical properties of spiral casing materials.

Material	Young Modulus [MPa]	Poisson coeff. [-]
Steel	210	0.27
Bronze	110	0.31
Composite: Epoxy Resin & Glass Fiber	38	0.28

For the 4 cross sections defined Figure 5, the corresponding value of the wave speed is calculated, see Figure 8. As expected for a constant spiral casing wall thickness the wave speed is increasing from the inlet up to the tongue as the cross section decreases. For the determination of the wave speed of the 19 elements of the spiral casing model a 2nd order polynomial interpolation is used, see Figure 8.
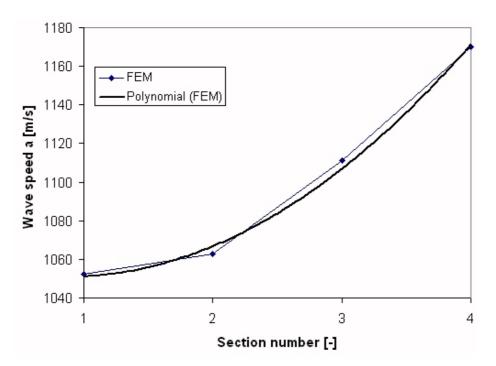

Figure **8** Wave speed evolution for the 4 cross sections of the spiral casing.

The wave speed of the distributor channels is found to be 800 m/s with small deviation between the 4 sections. The same value is chosen for the wave speed of the impeller blades.

Simulation of the Pump Turbine RSI

The pump turbine scale model of interest is installed on the test rig PF3 of the EPFL Laboratory for Hydraulic Machines. The hydroacoustic model of the test rig is including the pump turbine. A full description of the model of this test rig can be found in [16]. The test rig is made of 2 feedings pumps in series, a piping system, the pump turbine model itself and a downstream tank as presented Figure 9. The chosen operating condition for the simulation of the hydracoustic behavior of the test rig corresponds to the nominal operating point with no cavitation, a discharge of 0.23 m^3/s, a test head of 45 m and a rotational speed of 980 rpm. Each pipe of the spiral casing is considered as 1 element, and each guide vane and impeller vane is modeled with 3 elements. This spatial discretization ensures that a wavelength at the frequency $18 f_b$ ($k_1 = -2$) is represented by 20 elements. In agreement with the CFL criteria, an integration time step $dt = 85.034 \ \mu s$ corresponding to $0.5°$ of impeller rotation is selected. After convergence of the simulation to a periodic behavior, the simulation is continued for 10 impeller revolutions.
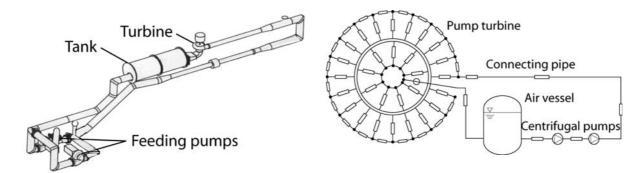

Figure 9 EPFL test rig PF3 and hydroacoustic model of the closed loop test rig N°3.

The resulting pressure fluctuations in the spiral casing and in the guide vanes close to the vaneless gap are properly non dimensionalized and presented in a waterfall diagram as a function of the dimensionless frequency f/f_b and the angular coordinate, see Figure 10. In these diagrams the angular origin is taken at the spiral casing inlet and therefore $\theta = 360°$ correspond to the tongue.

The pressure fluctuation in the vaneless gap, Figure 10, presents significant amplitudes for the expected frequencies $f/f_b = 9,\ 18,\ 27,\ 36,\ 45$, etc. and represents less than 0.5% of the head. The analysis of the phase, not presented here, of these pressure fluctuations shows clearly the diametrical pattern of the pressure mode shapes with for example 2 minima and 2 maxima, i.e. 4π phase shift, for the frequency of $f/f_b = 18$. The pressure fluctuations in spiral casing Figure 10 are characterized by a standing wave for the frequency $f/f_b = 18$ with a wavelength of approximately 4/3 of the spiral casing length. A pressure node is located at $\theta = 150°$ while amplitude maxima take place at $\theta = 20°$ and $\theta = 230°$. This standing wave influences the amplitude of the diametrical mode of the pressure fluctuation in the vaneless gap see Figure 10 .
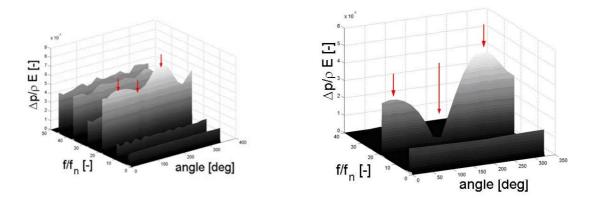

Figure 10 Waterfall diagram of the pressure fluctuations in the guide vanes close to the vaneless gap (left) and in the spiral casing (right).

Diametrical pressure mode k=-2

The patterns of the pressures fluctuations for $k_1 = -2$ are illustrated Figure 11. The representation is obtained by filtering the time signal of the pressure fluctuations of each spatial node in the pump turbine using a pass band filter around the frequency of interest. For the stationary frame it corresponds to $f/f_b = 18$. In the rotating frame it corresponds to $f/f_b = 20$. The pressure amplitude of every node of the pump turbine is represented on the z axis for the spatial position [x, y] of the node. The bold solid line is the connection between each last node of the guide vane and point out the diametrical mode shape pattern expected for $k_1 = -2$ with 2 maxima/minima. The diametrical mode rotates in the opposite direction of the impeller rotation as predicted by the analytical analysis above. The diametrical mode rotates with a spinning speed of $f_b = -9$. It means that using a pressure transducer in the vaneless gap, the frequency of $f/f_b = 18$ is measured. The interaction between the standing wave in the spiral casing and the diametrical mode are clearly pointed out through the pressure in the guide vanes where pressure fluctuations have similar amplitudes.
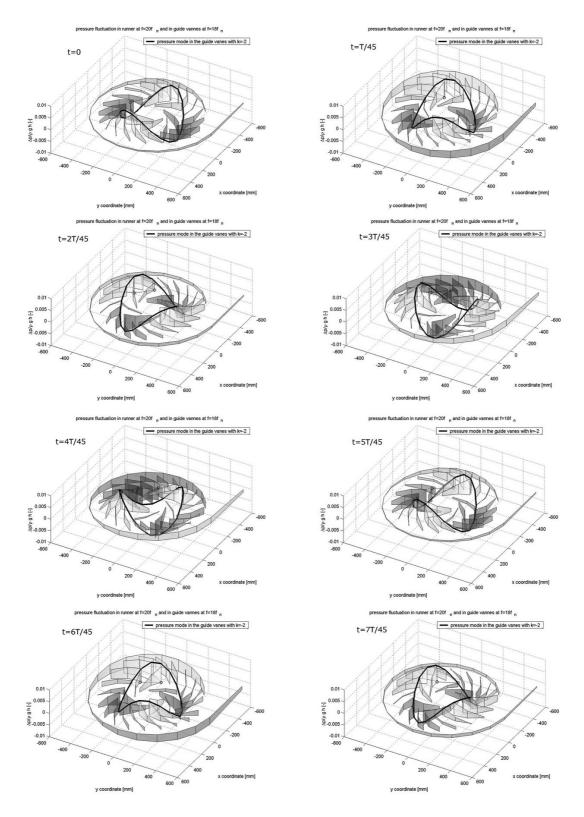
Figure 11 Pressure fluctuations patterns for $k_1 = -2$, $f/f_b = 18$ in the stationary part, $f/f_b = 20$ in the rotating part, from $t = 0$ to $t/T_b = 7/45$

Diametrical pressure mode k=-4

The patterns of the pressures fluctuations for $k_1 = -4$ are illustrated Figure 12. The representation is obtained by filtering the time signal of the pressure fluctuations of each spatial node in the pump turbine using a pass band filter around the frequency of interest. For the stationary frame it corresponds to $f/f_b = 36$. In the rotating frame it corresponds to $f/f_b = 40$. The pressure amplitude of every node of the pump turbine is represented on the z axis for the spatial position [x, y] of the node. The bold solid line is the connection between each last node of the guide vane and point out the diametrical mode shape pattern expected for $k_1 = -4$ with 4 maxima/minima. The diametrical mode rotates in the opposite direction of the impeller rotation as predicted by the analytical analysis above. The diametrical mode rotates with a spinning speed of $f_b = -9$. It means that using a pressure transducer in the vaneless gap, the frequency of $f/f_b = 36$ is measured. There is no standing wave in the spiral casing for this frequency.
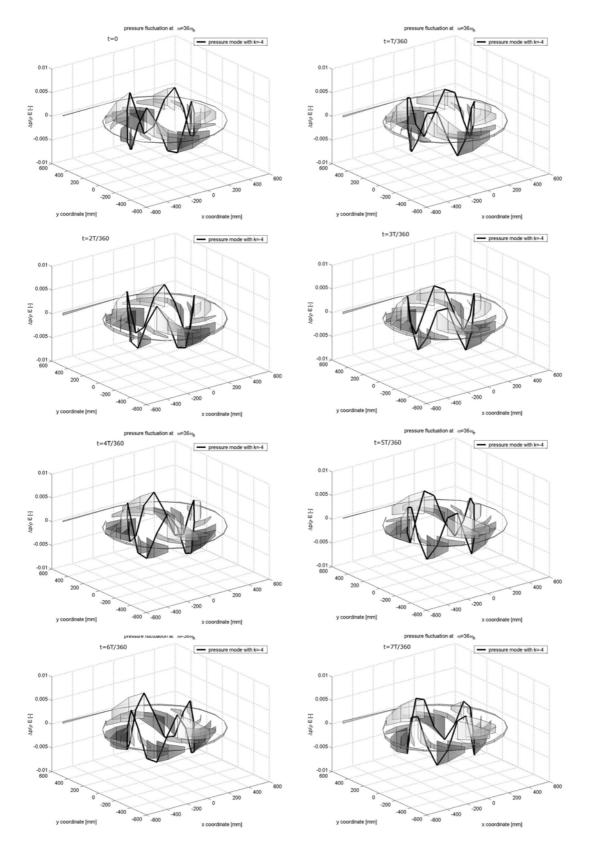
Figure 12 Pressure fluctuations patterns for $k_1 = -4$, $f/f_b = 36$ in the stationary part,

$f/f_b = 40$ in the rotating part, from $t = 0$ to $t/T_b = 7/45$

Diametrical pressure mode k=+5

The patterns of the pressures fluctuations for $k_1 = +5$ are illustrated Figure 13. The representation is obtained by filtering the time signal of the pressure fluctuations of each spatial node in the pump turbine using a pass band filter around the frequency of interest. For the stationary frame it corresponds to $f/f_b = 45$. In the rotating frame it corresponds to $f/f_b = 40$. The pressure amplitude of every node of the pump turbine is represented on the z axis for the spatial position [x, y] of the node. The bold solid line is the connection between each last node of the guide vane and point out the diametrical mode shape pattern expected for $k_1 = +5$ with 5 maxima/minima. The diametrical mode rotates in the same direction as the impeller. The diametrical mode rotates with a spinning speed of $f_b = +9$. It means that using a pressure transducer in the vaneless gap, the frequency of $f/f_b = 45$ is measured. There is no standing wave in the spiral casing for this frequency.
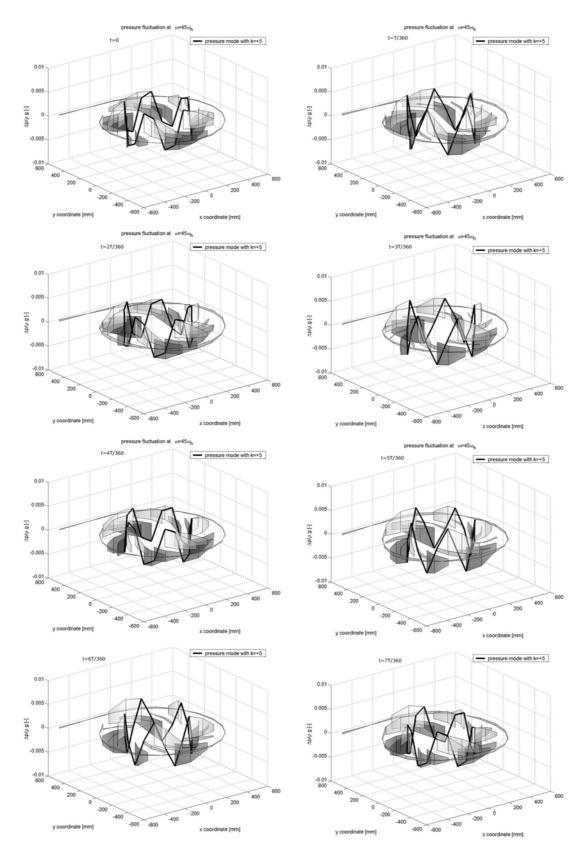
Figure 13 Pressure fluctuations patterns for $k_1 = +5$, $f/f_b = 45$ in the stationary part,

$f/f_b = 40$ in the rotating part, from $t = 0$ to $t/T_b = 7/45$

Diametrical pressure mode k=+7

The patterns of the pressures fluctuations for $k_1 = +7$ are illustrated Figure 14. The representation is obtained by filtering the time signal of the pressure fluctuations of each spatial node in the pump turbine using a pass band filter around the frequency of interest. For the stationary frame it corresponds to $f/f_b = 27$. In the rotating frame it corresponds to $f/f_b = 20$. The pressure amplitude of every node of the pump turbine is represented on the z axis for the spatial position [x, y] of the node. The bold solid line is the connection between each last node of the guide vane and point out the diametrical mode shape pattern expected for $k_1 = +7$ with 7 maxima/minima. The diametrical mode rotates in the same direction as the impeller. The diametrical mode rotates with a spinning speed of $f_b \cong +3.9$. It means that using a pressure transducer in the vaneless gap, the frequency of $f/f_b = 27$ is measured. There is no standing wave in the spiral casing for this frequency.
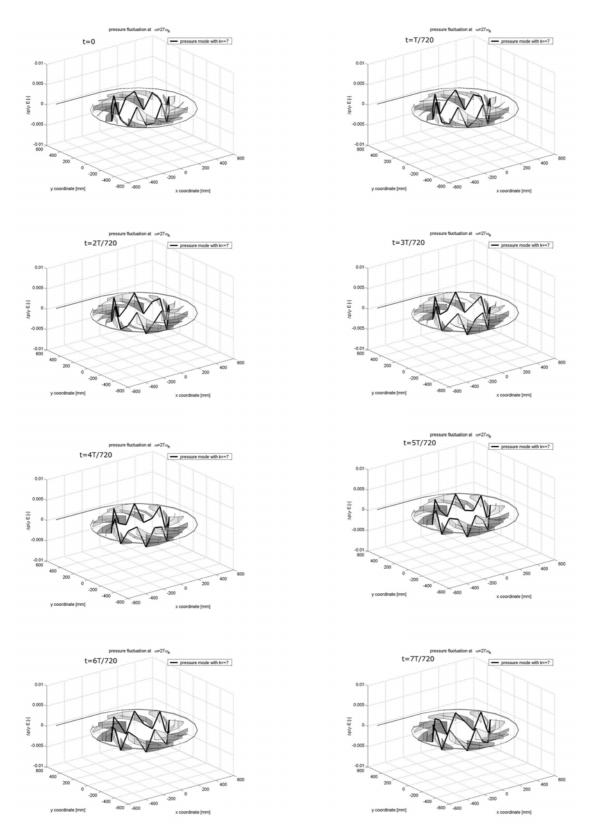
Figure 14 Pressure fluctuations patterns for $k_1 = +7$, $f/f_b = 27$ in the stationary part,

$f/f_b = 20$ in the rotating part, from $t = 0$ to $t/T_b = 7/45$

From these results it can be conclude that hydroacoustic model of the pump turbine allows to obtain and to visualize the RSI pressure fluctuation patterns. Standing wave and diametrical modes are pointed out and corresponding spinning speeds are properly obtained too. The high amplitude of the standing wave in the spiral casing for $k_1 = -2$ is probably related to a natural frequency of the hydraulic system which is close. However, it is important to notice that rotating impeller corresponds to unsteady boundary conditions at the end of the guide vanes. It makes the modal analysis difficult to be done by using linearized approaches. One of the major advantages of simulating the dynamic behavior of such a system in the time domain is that it offers the possibility to take into account such non-linearities. The modeling based on valve network driven accordingly by the flow distribution between stationary and rotating parts appears to be efficient for the simulation of the hydroacoustic part of the RSI phenomenon. This approach has the advantage to provide also the pressure fluctuations due to RSI in the rotating impeller.

Conclusion

Rotor stator interaction in Francis pump turbine may causes strong pressure fluctuations in the vaneless gap between the guide vanes and the impeller blades characterized by rotating diametrical mode shapes that can excite natural frequency of the hydraulic system and resulting in standing wave in the spiral casing. These 2 effects can induce resonance with mechanical or concrete structure jeopardizing the security of the power plant.

This paper presents a new approach for the modeling of the hydroacoustic part of the phenomenon. A one-dimensional simulation model of Francis pump turbine is set up according to the topology of a 20 guide vanes and 9 impeller vanes pump turbine. The hydroacoustic parameters of the model are determined from the geometrical and structural characteristics of the machine and the test rig.

The resulting RSI model comprises a network of 180 valves connecting each guide vane with each impeller vane. The valve opening functions are driven accordingly with the flow distribution between the stationary part and the rotating parts. The analysis of the pressure fluctuations resulting from the rotor stator excitation shows that RSI patterns like rotating diametrical pressure mode and standing wave are properly simulated. Influence of the standing wave on the diametrical pressure mode is pointed out. The chosen excitation model appears to be realistic for the investigation of hydroacoustic part of the RSI.

Overall, this model gives satisfactory qualitative results and needs to be validated experimentally. However, if the dynamic amplification gives reliable trends, the determination of the absolute pressure fluctuations amplitudes is more challenging. The excitation model is based on the flow distribution between the stationary parts and the rotating parts of the machine and is arbitrary. Its parameters are only related to connection area between guide vanes and impeller blades evolution due to impeller rotation. To obtain a more reliable quantitative result, the excitation model should be improved and be able to take into consideration all the parameters affecting RSI like the gap amplitude, the wake angle of the impeller blade and the blades thickness etc. This could be achieved through the coupling of a one-dimensional code like SIMSEN for the modeling of the hydraulic system with a CFD tool for the modeling of the RSI excitation. This approach seems realistic regarding the negligible influence of the impeller hydroacoustic parameters.

Appendix. Nomenclature

Nomenclature

A Cross Section Area (m^2)

C Absolute Mean Flow Speed (m/s), $C = Q/A$

C_h Hydraulic Capacitance (m^2), $C_h = gA/a^2$

D Pipe diameter (m)

E Young Modulus (Pa)

E Machine Specific Energy (J/kg), $E = gH_1 - gH_2$

H Head (m), $H = E/g$

L_h Hydraulic Inductance (s^2/m^2), $L_h = dx/gA$

Q Flow rate, (m^3/s) $Q = C \cdot A$

R_h Hydraulic Resistance (s/m^2), $R_h = \lambda dx |Q| / 2gDA^2$

R_{ref} Machine Reference Radius (m)

h Piezometric Head (m), $h = p/\varpi + Z$

a Wave Speed (m/s)

f_b Impeller Rotational Frequency (Hz)

p Pressure (Pa)

g Gravity Acceleration (m/s^2)

ρ Water Density, (kg/m^3)

φ Discharge Coefficient, $\varphi = Q / \pi\omega R_{ref}^3$

ψ Specific Energy Coefficient, $\psi = 2E / \omega^2 R_{ref}^2$

ν Machine Specific Speed, $\nu = \varphi^{1/2} / \psi^{3/4}$

λ Local Loss Coefficient

ω_b Impeller Angular Speed (rad/s)

n Harmonic Order

m Harmonic Order

z_o Number of Guide Vanes, $z_o = 20$

z_b Number of impeller blades, $z_b = 9$

θ_s Angle in the Stationary System

θ_r Angle in the Rotating System

B_n Amplitude for the nth Harmonic (Pa)

B_m Amplitude for the mth Harmonic (Pa)

ϕ_n Phase for the nth Harmonic

ϕ_m Phase for the mth Harmonic

REFERENCES

[1]   Bolleter, U., 1988, "Blade passage tones of centrifugal pump. ", Vibrations, Vol. 4, No 3, pp. 8-13.

[2]   Ohura, Y., Fujii, M., Sugimoto, O., Tanaka, H., Yamagata, I., 1990, "Vibration of the powerhouse structure of pumped storage power plant.", Proceedings, 15th IAHR Symposium, Belgrade, section U2.

[3]   Chen, Y. N., 1961, "Water-Pressure Oscillations in the Volute Casings of Storage Pumps.", Sulzer Technical Review, Research Number, pp. 21-34.

[4]   Dörfler, P., 1984, "On the phase role of phase resonance in vibrations caused by blade passage in radial hydraulic turbomachines.", Proceedings, 12th IAHR Symposium, Stirling, paper 3.3, pp. 227-241.

[5]   Tanaka, H., 1990, "Vibration behaviour and dynamic stress of runners of very high head reversible pump-turbines." Proceedings, 15th IAHR Symposium, Belgrade, Yugoslavia.

[6]   Fischer, R., Powell, C., Franke, G., Seidel, U., Koutnik, J., 2004, "Contributions to the improved understanding of the dynamic behavior of pump turbines and uses thereof in dynamic design.", Proceedings, 22nd IAHR Symposium, Stockholm, paper B11-3.

[7]   Den Hartog, J. P., 1956, "Mechanical vibrations.", 4th edition, New York, McGraw-Hill pp. 7-9.

[8]   Haban, V., Koutnik, J., Pochyly, F., 2002, "1-D Mathematical model of high-frequency pressure oscillations induced by RSI including an influence of fluid second viscosity.", Proceedings, 21st IAHR Symposium, Lausanne, pp. 735-740.

[9]   Gonzalez, J., Fernandez, J., Blanco, E., Santolaria, C., 2002, "Numerical simulation of the dynamic effects due to impeller-volute interaction in a centrifugal pump. ", Trans. ASME, J. Fluids Eng., vol. 124, pp. 348-355, June 2002.

[10]   Moregenroth, M., Weaver, D. S., 1998, "Sound generation by a centrifugual pump at blade passing frequency", ASME, J. Fluids Eng. Vol. 120, pp. 736-743, October 1998.

[11]   Parrondo-Gayo, J. L., Gonzalez-Perez, J., Fernandez-Franco, 2002, "The effect of the operating point on the pressure fluctuations at blade passage frequency in the volute of a centrifugal pump. ", Trans. ASME, J. Fluids Eng., vol. 124, pp. 348-355, September 2002.

[12]   Franke, G., Powell, C., Seidel, U., Koutnik, J., Fischer, R., 2005, "On pressure mode shapes arising from rotor/stator interactions.", Sound & Vibration, March 2005, pp. 14-18.

[13]   Wylie, E. B. & Streeter, V.L., 1993, "Fluid transients in systems". Prentice Hall, Englewood Cliffs, N.J.

[14]   Paynter, H. M., 1953 "Surge and water hammer problems". Transaction of ASCE, vol. 146, p 962-1009.

[15]   Nicolet, C., Avellan, F., Allenbach, P., Sapin, A., Simond, J.-J., 2002, "New Tools for the Simulation of Transient Phenomena in Francis Turbine Power Plants". Proceedings of the 21st IAHR Symposium, Lausanne, pp. 519-528.

[16]   Nicolet, C. , Arpe, J., Avellan, F., 2004 "Identification and Modeling of Pressure Fluctuations of a Francis Turbine Scale Model at Part Load Operation ". Proceedings of the 22nd IAHR Symposium on Hydraulic Machinery and Systems, Stockholm, Sweden.